

Article

The Data-Driven Optimization Method and Its Application in Feature Extraction of Ship-Radiated Noise with Sample Entropy

Yuxing Li ^{1,*} , Xiao Chen ², Jing Yu ³ , Xiaohui Yang ^{4,*}  and Huijun Yang ⁵

¹ Faculty of Information Technology and Equipment Engineering, Xi'an University of Technology, Xi'an 710048, Shaanxi, China

² College of Electrical & Information Engineering, Shaanxi University of Science & Technology, Xi'an 710021, Shaanxi, China; chenxiao@sust.edu.cn

³ School of Marine Science and Technology, Northwestern Polytechnical University, Xi'an 710072, Shaanxi, China; yujing@nwpu.edu.cn

⁴ School of Art and Design, Inner Mongolia University of Science & Technology, Baotou 014010, Inner Mongolia, China

⁵ College of Information Engineering, Northwest A&F University, Yang'ling 712100, Shaanxi, China; yhj740225@nwsuaf.edu.cn

* Correspondence: liyuxing@xaut.edu.cn (Y.L.); yxh198715@163.com (X.Y.)

Received: 28 December 2018; Accepted: 21 January 2019; Published: 23 January 2019



Abstract: The data-driven method is an important tool in the field of underwater acoustic signal processing. In order to realize the feature extraction of ship-radiated noise (S-RN), we proposed a data-driven optimization method called improved variational mode decomposition (IVMD). IVMD, as an improved method of variational mode decomposition (VMD), solved the problem of choosing decomposition layers for VMD by using a frequency-aided method. Furthermore, a novel method of feature extraction for S-RN, which combines IVMD and sample entropy (SE), is put forward in this paper. In this study, four types of S-RN signals are decomposed into a group of intrinsic mode functions (IMFs) by IVMD. Then, SEs of all IMFs are calculated. SEs are different in the maximum energy IMFs (EIMFs), thus, SE of the EIMF is seen as a novel feature for S-RN. To verify the effectiveness of the proposed method, a comparison has been conducted by comparing features of center frequency and SE of the EIMF by IVMD, empirical mode decomposition (EMD) and ensemble EMD (EEMD). The analysis results show that the feature of S-RN can be obtained efficiently and accurately by using the proposed method.

Keywords: data-driven; variational mode decomposition (VMD); improved variational mode decomposition (IVMD); empirical mode decomposition (EMD); feature extraction; sample entropy (SE); ship-radiated noise (S-RN)

1. Introduction

The data-driven method is an effective research method in both scientific research and practical applications [1–3]. The complexity of the ocean background makes it hard to obtain the features of ship radiated noise (S-RN) [4–6]. The existing feature extraction methods based on Fourier analysis are not suitable for underwater acoustic signals [7]. The empirical mode decomposition (EMD) is a kind of data-driven and self-adaptive signal decomposition method for non-linear and non-stationary signal [8–10]. Due to the mode mixing of EMD, ensemble EMD [11] was put forward after EMD, which inhibits this phenomenon to some extent by adding noise. Still, EEMD and other improved EMD methods are all empirical ones without mathematical derivation [12].

With the development of data-driven methods, some more effective methods have been proposed. In 2014, to avoid the aforementioned problems of EMD, variational mode decomposition (VMD) was employed as a novel kind of data-driven signal analysis tool, which has better decomposition performance and robustness to noise than improved EMD methods [13]. In reference [14], several different data-driven methods are compared, including empirical wavelet transform, VMD, Vold–Kalman filter order tracking, EMD and its four kinds of improved methods. In reference [15], three underwater acoustic signals denoising methods are compared based on EMD, EEMD and VMD respectively, the results show that the VMD-based denoising methods are superior to other EMD-based and EEMD-based denoising methods. Meanwhile, the VMD-based feature extraction methods for underwater acoustic signal also have better performance [16].

In recent years, the two kinds of data-driven decomposition methods have developed rapidly. On the one hand, the existing theoretical problems of themselves have been addressed; on the other hand, their application areas have also been expanded. Some modified EMD methods have been proposed to inhibit mode mixing; unfortunately, they are all empirical methods. To overcome the influence of the parameter selection problem in VMD, some modified VMD methods are put forward, which are suitable for analyzing different kinds of signals, such as magnetocardiography (MCG) [17] and bearing signals [18]. The application of VMD in underwater acoustic field is very limited. To solve the parameter selection problem of VMD, the existing methods depend on engineering experience or are based on EMD assistant selection. However, we have not found a modified VMD method for underwater acoustic signals.

Sample entropy (SE) [19], like permutation entropy (PE), has the ability to explain the complexity of time series. Unlike PE [20,21], SE represents complexity by measuring the probability of new patterns, which have high reliability and consistency for data of different lengths. The method based on mode decomposition and entropy has been applied in many aspects, such as fault diagnosis [22–24], medical science [25] and other fields [26–28]. In reference [22], EEMD and PE are used in bearing fault diagnosis. In reference [28], EEMD and SE are employed in feature extraction of partial discharge. In underwater acoustic field, PE is first used to extract S-RN feature by EMD [26]. However, only three types of S-RN are applied, and SE is seldom used to analyze the complexity of underwater acoustic signals.

In this paper, IVMD, as a new data-driven method, is first put forward to solve the problem of choosing parameters for VMD by using frequency-aided method. Then, we proposed a novel feature extraction method for S-RN based on IVMD and SE. For underwater acoustic signal processing, feature extraction using IVMD and SE is seldom discussed. In Section 2, IVMD and the novel feature extraction methods are described; the SE and center frequency of all IMFs are compared and analyzed by IVMD, EMD and EEMD in Section 3; the SE of the maximum energy IMF (EIMF) is seen as a novel feature and compared with other methods in Section 4; the last Section is the conclusion.

2. Theoretical Framework

2.1. VMD

As a data-driven signal decomposition method, VMD can decompose the target signal into a group of IMFs. Unlike the IMF definition of EMD, VMD defines IMF as Amplitude Modulation Frequency Modulation (AM-AF) signal, which has frequency center and limited bandwidth by solving the non-constrained variational model, as follows:

$$L(\{u_k\}, \{w_k\}, \lambda) = \alpha \sum_{k=1}^K \left\| \partial_t \left[(\delta(t) + \frac{j}{\pi t}) \times u_k(t) \right] e^{-jw_k t} \right\|_2^2 + \left\| x(t) - \sum_{k=1}^K u_k(t) \right\|_2^2 + \left\langle \lambda(t), x(t) - \sum_{k=1}^K u_k(t) \right\rangle \quad (1)$$

Table 1 lists the mathematical symbols of the non-constrained variational model. Alternating direction multiplier method is used to obtain the saddle points, then we can update \hat{u}_k^{n+1} , w_k^{n+1} and $\hat{\lambda}^{n+1}$ according to Equation (2).

Table 1. Mathematical symbols of the non-constrained variational model.

L	α	λ	K	$u_k(t)$	$x(t)$	w_k
Augmentd Lagrangian	Penalty factor	Lagrange multiplier	Number of IMF	k -th IMF	Target signal	Estimated frequency

$$\begin{cases} \hat{u}_k^{n+1}(w) = \frac{\hat{x}(w) - \sum_{i < k} \hat{u}_i^n(w) - \sum_{i > k} \hat{u}_i^n(w) + \frac{\hat{\lambda}^n(w)}{2}}{1 + 2\alpha(w - w_k^n)^2} \\ w_k^{n+1} = \frac{\int_0^\infty w |\hat{u}_k^{n+1}|^2 dw}{\int_0^\infty |\hat{u}_k^{n+1}|^2 dw} \\ \hat{\lambda}^{n+1}(w) = \hat{\lambda}^n(w) + \tau \left(\hat{x}(w) - \sum_k \hat{u}_k^{n+1}(w) \right) \end{cases} \quad (2)$$

where w represents frequency domain. The process of VMD is as follows:

- (1) Make \hat{u}_k^1, w_k^1 and $\hat{\lambda}^1$ and n equal to 0.
- (2) $n = n + 1$. Update $\hat{u}_k^{n+1}, w_k^{n+1}$ and $\hat{\lambda}^{n+1}$ by using Equation (2).
- (3) Repeat step 2 until the end condition is met as follows:

$$\sum_k \left\| \hat{u}_k^{n+1} - \hat{u}_k^n \right\|_2^2 / \left\| \hat{u}_k^n \right\|_2^2 < e \quad (3)$$

More detailed instructions are available in reference [13].

The differences between IVMD, VMD, EMD and EEMD are as follows:

- (1) EMD, EEMD and other EMD-based improved algorithms are all empirical data-driven decomposition methods, however, VMD and IVMD are not empirical algorithms and based on a foundation of mature mathematical theories and methods, which are wiener filtering, Hilbert transform, analytic signal and heterodyne demodulation.
- (2) The sensitivity of VMD and IVMD to noise is lower than that of EMD, EEMD and other improved EMD algorithms.
- (3) Based on the above two points, VMD and IVMD have better decomposition performance than EMD and EEMD. In addition, IVMD, as an improved method of VMD, solved the problem of choosing decomposition layers for VMD by using the frequency-aided method.

2.2. IVMD

In order to better analyze S-RN signals, a frequency-aided VMD method, called IVMD, is proposed. IVMD mainly solves the problem of choosing decomposition layers for VMD. The processing of VMD has been expressed in many studies. Therefore, here we focus on the IVMD approach as follows:

- (1) Because of the complexity of S-RN, we initialize $K = 5$ according to EMD results.
- (2) Decompose S-RN to obtain K IMFs and corresponding center frequency by VMD.
- (3) Make $K = K + 1$.
- (4) We can also obtain K IMFs and corresponding center frequency by VMD.
- (5) Determine the new center frequency. When K increases by 1, we get a new center frequency. For example, when $K = n + 1$, compare the $n + 1$ center frequencies with the center frequencies obtained under $K = n$, find the nearest center frequencies, calculate the frequency difference separately, and regard the maximum frequency difference as the new center frequency.
- (6) Judge whether or not the decomposition is excessive. We make the new center frequency equal to A ($K = n + 1$), the center frequency nearest to A is B ($K = n$). When $A \in [0.85B, 1.15B]$, the decomposition is excessive, we make $K = n - 1$. When $A \notin [0.85B, 1.15B]$, we repeat steps from (3) to (6) until $A \in [0.85B, 1.15B]$.

(7) Process S-RN by VMD with the decomposition layer K .

2.3. SE

Data of length N constitutes time series $\{x(n)\} = x(1), x(2), \dots, x(n)$, the steps of SE are as follows [11]:

- (1) $\{x(n)\}$ is reconstructed into a set of vector sequences $X_m(1), X_m(1+m), X_m(1+2m), \dots, X_m(N-m+1)$ with dimension m .
- (2) Define the distance between $X_m(i)$ and $X_m(j)$ as follows:

$$d[X_m(i), X_m(j)] = \max(|x(i+k) - x(j+k)|) \quad (4)$$

- (3) Set a tolerance threshold to r , the number of $d[X_m(i), X_m(j)] \leq r$ is B_i ($i \neq j$). $B_i^m(r)$ can be expressed as follows:

$$B_i^m(r) = \frac{1}{N-m-1} B_i, (1 \leq i \leq N-m) \quad (5)$$

- (4) The mean value of $B_i^m(r)$ can be expressed as follows:

$$B^m(r) = \frac{1}{N-m} \sum_{i=1}^{N-m} B_i^m(r) \quad (6)$$

- (5) $B^{m+1}(r)$ can be obtained by increasing dimension m to $m+1$.
- (6) Finally, SE can be defined as follows:

$$\text{SampEn}(m, r, N) = -\ln \left[\frac{B^{m+1}(r)}{B^m(r)} \right] \quad (7)$$

More detailed instructions are available in reference [19].

2.4. Feature Extraction Based on IVMD and SE

IVMD has a strong ability of analysis in the time-frequency domain. Combined with the property of the SE, a new feature extraction approach can be designed as shown in Figure 1. The main steps are as follows:

Step 1: The four types of S-RN signal are sampled and then normalized. Also, some parameters of IVMD were compared and selected. Then, we can obtain all the IMFs components by EMD, EEMD and IVMD.

Step 2: The order of IMF was reordered by center frequency and energy descending respectively, and the center frequency and SE of each arranged IMF was calculated. After analysis and comparison, the optimal IMF was chosen to represent the original signal.

Step 3: Calculate the center frequency and SE of 20 optimal IMFs for each type, and then analysis the statistic characteristic parameters of S-RN signal. Compare with feature extraction methods by IVMD, EMD and EEMD, we can select one optimal feature which is easy to use to distinguish the four types of S-RN signals.

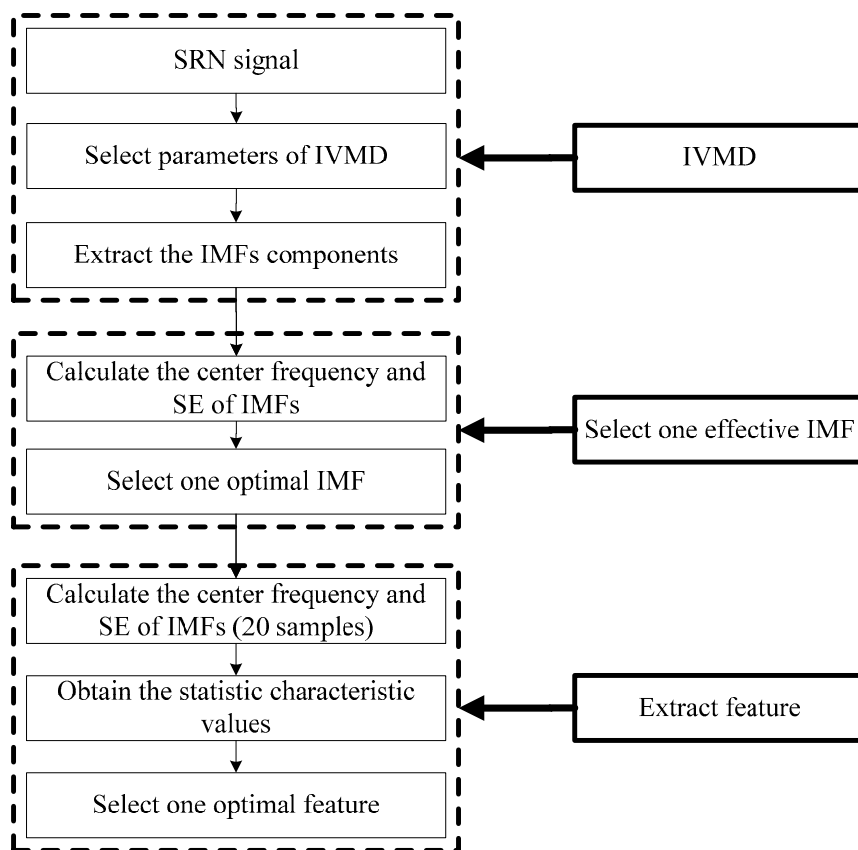


Figure 1. Flow chart of proposed feature extraction method.

3. Simulations and Experiments Evaluation

3.1. The Selection of IVMD Parameters

The selection of IVMD parameters is often not the same for different kinds of signals. Three main parameters are involved in VMD, namely, number of mode K , initial condition and quadratic penalty α . In this paper, four types of S-RN signal are simulated all signal types are the same as the signal in reference [26], with the exception of the first type of S-RN signal. Four types of S-RN samples are normalized to get the time-domain waveform shown in Figure 2, their sampling frequency is 44.1 kHz, and the data length of samples is 5000.

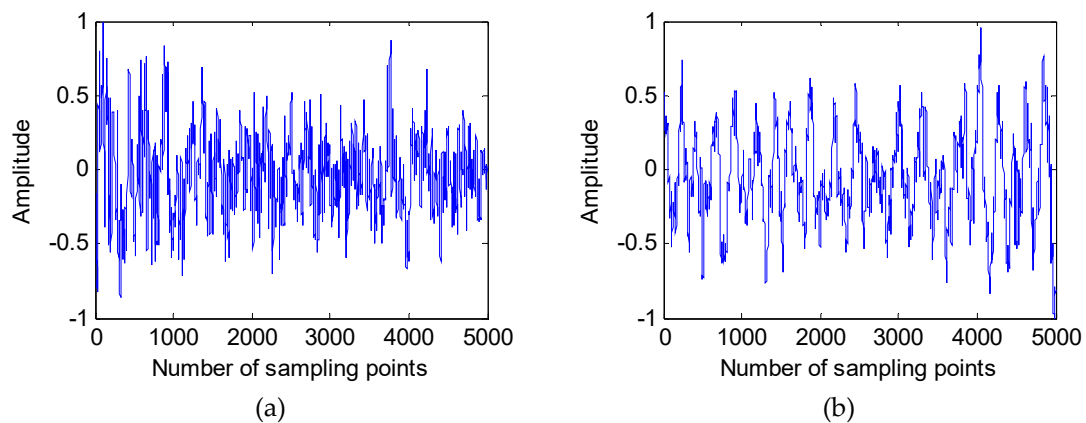


Figure 2. Cont.

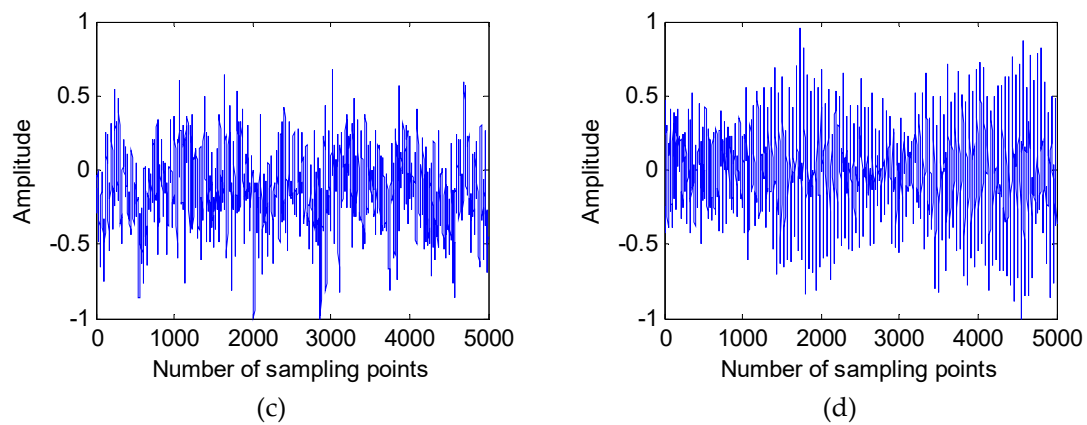


Figure 2. The time-domain waveform for four types of S-RN signals. (a) The first S-RN; (b) The second S-RN; (c) The third S-RN; (d) The fourth S-RN.

The number of mode K could be take 5 to 9, in order to better observe the center frequency distribution of the four types of S-RN signals by IVMD, the center frequency is arranged in ascending order, as shown in Table 2. When the K is increased by 1, a new IMF will be generated, then a new center frequency with large difference from the original center frequency is obtained with a red mark. According to the over-decomposition rules, when $K = 9$, the decomposition for four types of S-RN signals is excessive except for the second one. While the new center frequency of the second type of S-RN signals belong to high-frequency which has little influence on feature extraction of the S-RN signal. Therefore, for the convenience in analyzing this paper makes $K = 8$.

Table 2. (a) Results of IVMD for the first S-RN. (b) Results of IVMD for the second S-RN. (c) Results of IVMD for the third S-RN. (d) Results of IVMD for the fourth S-RN.

	K	Center Frequency/Hz								
(a)	5	188.53	849.53	1509.2	2193.5	3624.4				
	6	187.49	838.22	1478.6	1978.3	2833.8	3986.8			
	7	186.94	833.06	1466.4	1885.4	2477.3	3424.1	4453.4		
	8	186.73	831.21	1462.2	1859.4	2397.5	3266.4	4159.9	5760.3	
	9	186.23	826.66	1451.7	1796.1	2210.6	2754.3	3504.3	4349.4	5918.8
(b)	5	164.74	553.38	1021.1	1946.4	3172.5				
	6	164.65	549.79	1002.2	1856	2902.4	4315.3			
	7	164.18	527.69	886.41	1324.9	2063.2	3081.1	4631.5		
	8	164.18	527.5	885.65	1322.9	2058.7	3066.6	4540.9	12980	
	9	164.17	526.79	882.7	1314.4	2036.7	2988.5	4120.7	6253.8	12991
(c)	5	32.395	799.51	1554.6	2641.9	3889				
	6	31.876	796.34	1507.5	2487.2	3169.9	4143.5			
	7	31.766	796.17	1503.9	2477.9	3127.9	3989	4985.3		
	8	31.687	795.88	1500.1	2471.7	3107.7	3942.1	4771.3	6722.4	
	9	29.988	784.96	1256.9	1702.7	2515	3139.2	3962	4801.4	6737.5
(d)	5	205.38	648.2	972.45	2190.8	4032.7				
	6	176.42	636.42	969.22	2046.6	3164.8	4925.1			
	7	148.28	619.95	969.56	2035.6	3126.2	4805.1	7833.6		
	8	127.58	601.48	967.98	2011.8	2966.1	3925.5	5099.1	7980.4	
	9	125.62	596.18	967.26	1856.7	2263.7	3013.2	3946.3	5114.6	7997.8

Keep $K = 8$ constant, the simulation experiments are carried out under the conditions of zero initial and uniformly spaced distribution, the center frequency distribution of four types of S-RN signals is shown in Table 3. For two different initial conditions, the center frequency distribution of the first and second type are very close, there is a big difference between the high-frequency for the third type, and the center frequency distribution of the fourth type in high-frequency and low-frequency were significantly different. For the S-RN signal, the main energy is concentrated in the low frequency part, which is also the key to distinguishing the different ships. Therefore, when $K = 8$, the zero initial is chosen as the initial condition.

Table 3. (a) Results of IVMD for the first S-RN. (b) Results of IVMD for the second S-RN. (c) Results of IVMD for the third S-RN. (d) Results of IVMD for the fourth S-RN.

	Initial	Center Frequency/Hz							
(a)	Zero initial	186.73	831.2	1462.2	1859.4	2397.5	3266.4	4159.9	5760.3
	Uniformly distribution	186.81	832.09	1464.5	1871.6	2428.2	3309.9	4209	5806.4
	Initial	Center Frequency/Hz							
(b)	Zero initial	164.18	527.5	885.65	1322.9	2058.7	3066.6	4540.9	12980
	Uniformly distribution	164.62	548.78	998.46	1842.1	2870.1	4237.5	11689	13246
	Initial	Center Frequency/Hz							
(c)	Zero initial	31.687	795.88	1500.1	2471.7	3107.7	3942.1	4771.3	6722
	Uniformly distribution	31.788	796.13	1504.6	2482.4	3152.8	4092	6357.1	11885
	Initial	Center Frequency/Hz							
(d)	Zero initial	127.58	601.48	967.98	2011.8	2966.1	3925.5	5099.1	7980.4
	Uniformly distribution	945.19	1935.5	2914.5	3874.6	4996.2	7485.8	9940.9	12368

When the initial condition is zero initial and $K = 8$, the influence of the quadratic penalty is studied under different order of magnitude. As shown in Table 4, it is found that with the increase of the penalty factor, the center frequency of the four types decreases gradually and the overall range of center frequency become small. When the penalty factor is 2×10^4 , the highest center frequency cannot reflect the actual frequency characteristics of the S-RN signal, therefore, 2×10^3 is regarded as the penalty factor.

Table 4. (a) Results of IVMD for the first S-RN. (b) Results of IVMD for the second S-RN. (c) Results of IVMD for the third S-RN. (d) Results of IVMD for the fourth S-RN.

	Penalty Factor	Center Frequency/Hz							
(a)	2×10^2	192.28	881.84	1550.5	2306.2	3440	4570.5	6965.9	10783
	2×10^3	186.73	831.2	1462.2	1859.4	2397.5	3266.4	4159.9	5760.3
	2×10^4	111.57	258.56	471.52	856.82	1140.4	1520.6	1931.8	2599.1
	Penalty Factor	Center Frequency/Hz							
(b)	2×10^2	166.23	602.2	1180.2	2088.5	3440.1	5406.1	9662.2	12932
	2×10^3	164.18	527.5	885.65	1322.9	2397.5	3066.6	4540.9	12980
	2×10^4	35.641	170.8	278.36	573.36	915.54	1300.1	1922.2	2466.1
	Penalty Factor	Center Frequency/Hz							
(c)	2×10^2	34.145	803.63	1595.7	2666.4	3859.7	5752.7	8733.2	12336
	2×10^3	31.687	795.88	1500.1	2471.7	3107.7	3942.1	4771.3	6722
	2×10^4	14.905	379.92	798.22	950.56	1325.6	1683.4	2548.9	3245.9
	Penalty Factor	Center Frequency/Hz							
(d)	2×10^2	933.83	1886.1	2891.6	3893.4	5142.3	7515.8	9916.8	12458
	2×10^3	127.58	601.48	967.98	2011.8	2966.1	3925.5	5099.1	7980.4
	2×10^4	110.41	455.21	638.25	960.53	973.68	1238.1	1732.9	2116.8

3.2. The IVMD of S-RN

Simulations are conducted to compare the result of EMD, EEMD and IVMD for four types of S-RN signal. Normalized samples for each type are recorded. Figures 3–5 show the results of EMD, EEMD and IVMD for the four types of S-RN signal respectively, while Figures 6–8 represent the corresponding IMF spectrum distribution (frequency less than 15,000 Hz).

The decomposition by EMD and EEMD is from high to low frequency, for comparison purposes, IMFs by IVMD are rearranged in the center frequency descending order. By observing Figures 3–5, it can be found that when the number of IMF by EEMD is more than by EMD, the two methods both show adaptive decomposition, while when IVMD uses the selected $K = 8$, the number of IMF is consistent. Figures 6–8 indicate that the IMF obtained by EMD and EEMD have a wide bandwidth, especially the high-frequency IMF, while the IMF obtained by the IVMD method has a narrow bandwidth, which is beneficial to the feature extraction of S-RN signal.

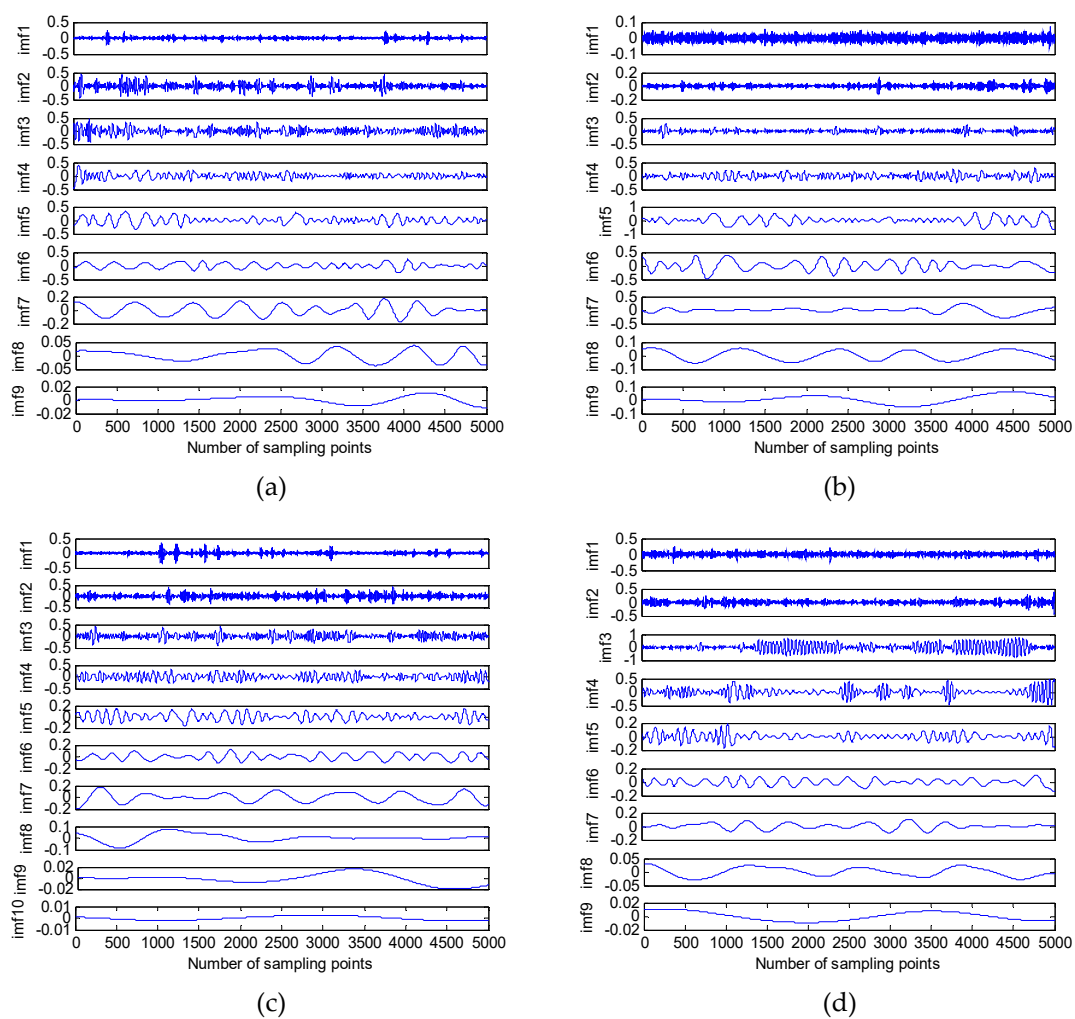


Figure 3. The result of EMD for four types of S-RN signals. (a) The first S-RN; (b) The second S-RN; (c) The third S-RN; (d) The fourth S-RN.

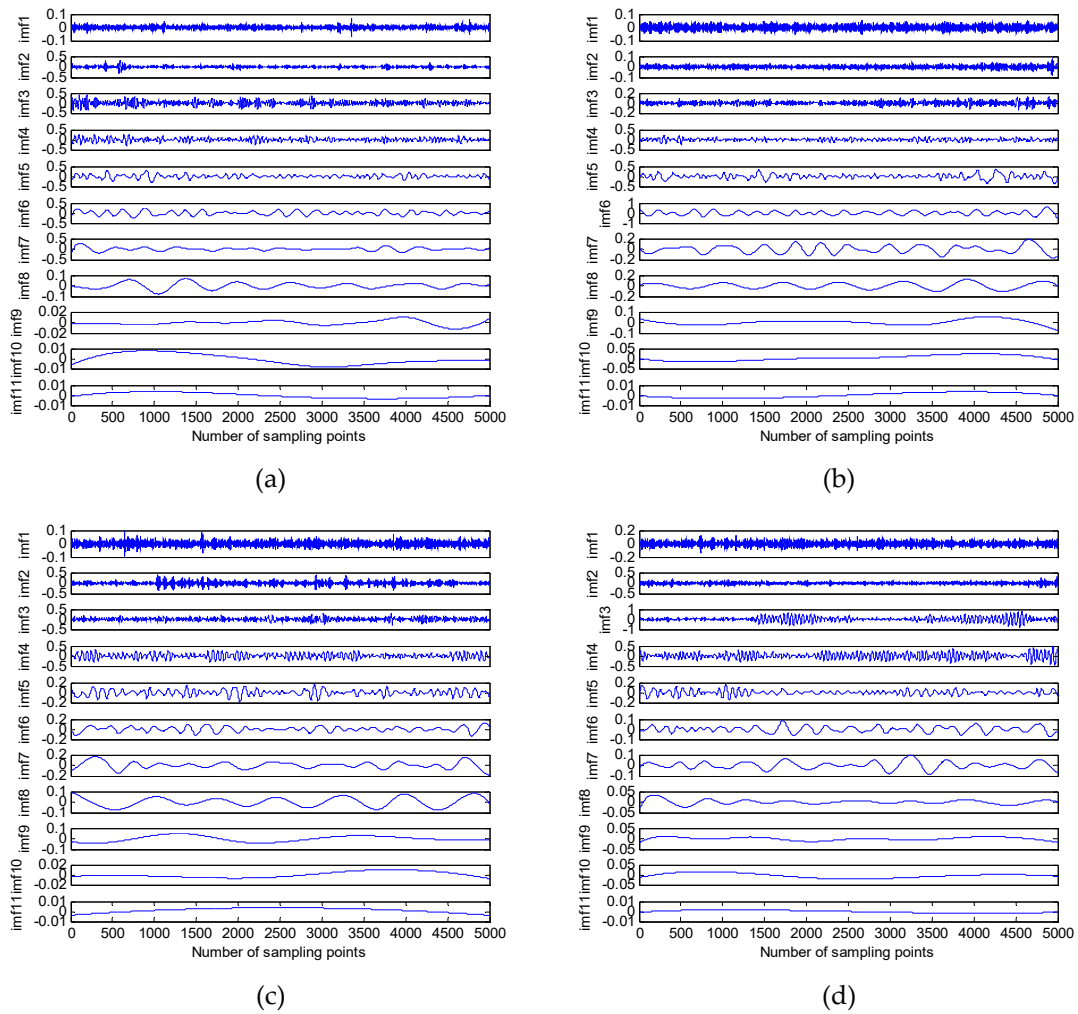


Figure 4. The result of EEMD for four types of S-RN signals. (a) The first S-RN; (b) The second S-RN; (c) The third S-RN; (d) The fourth S-RN.

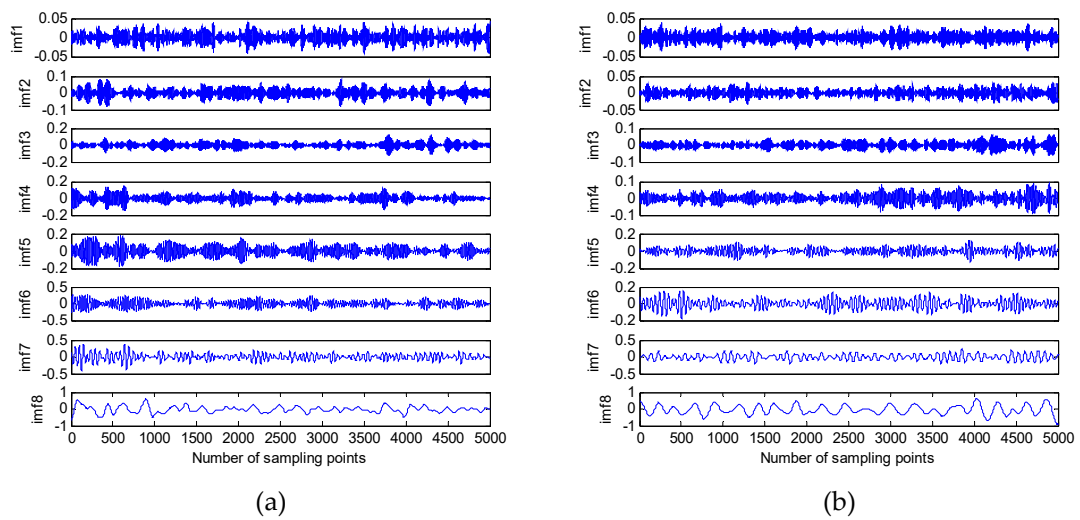


Figure 5. Cont.

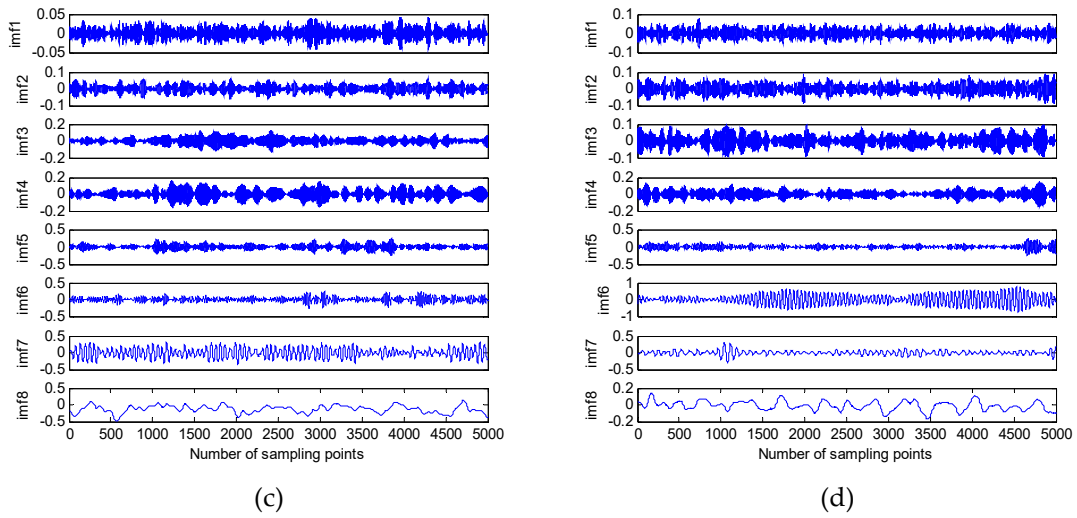


Figure 5. The result of IVMD for four types of S-RN signals. (a) The first S-RN; (b) The second S-RN; (c) The third S-RN; (d) The fourth S-RN.

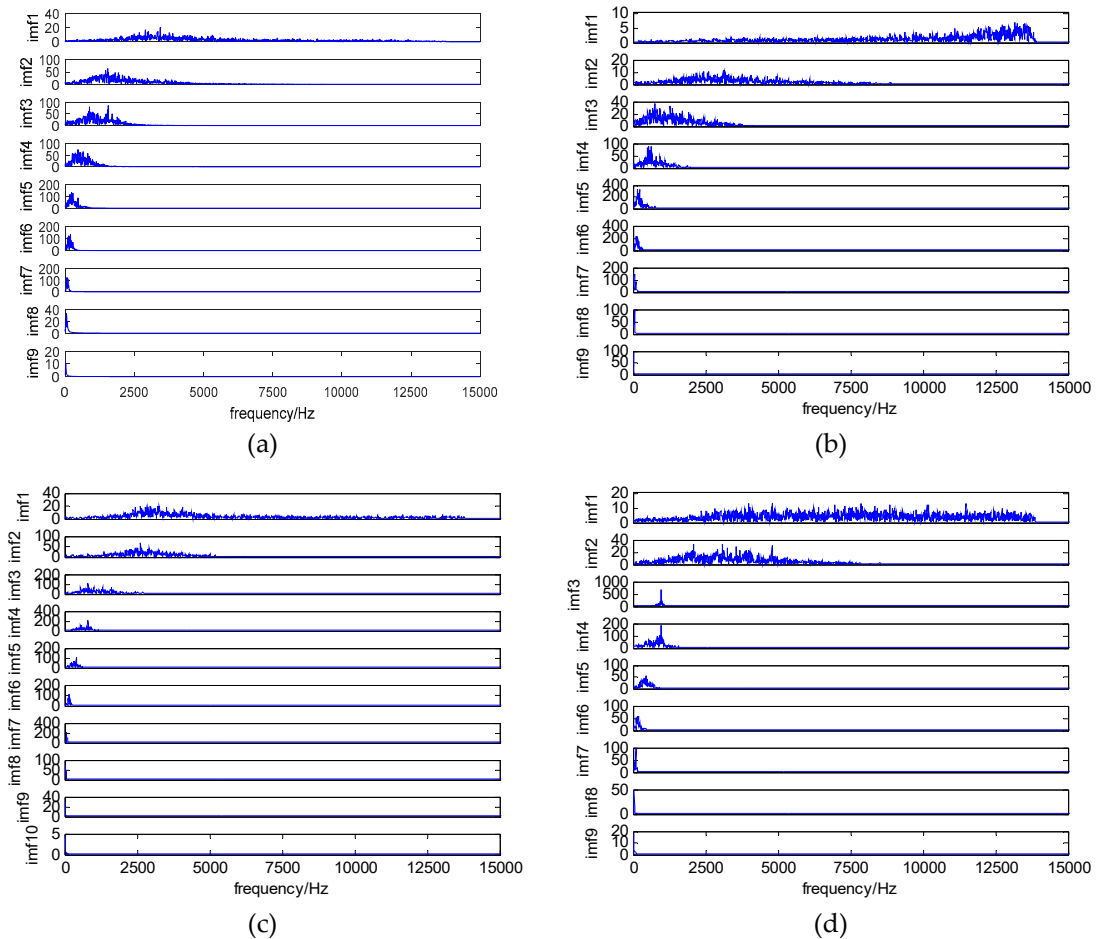


Figure 6. The IMF spectrum distribution by EMD for four types of S-RN signals. (a) The first S-RN; (b) The second S-RN; (c) The third S-RN; (d) The fourth S-RN.

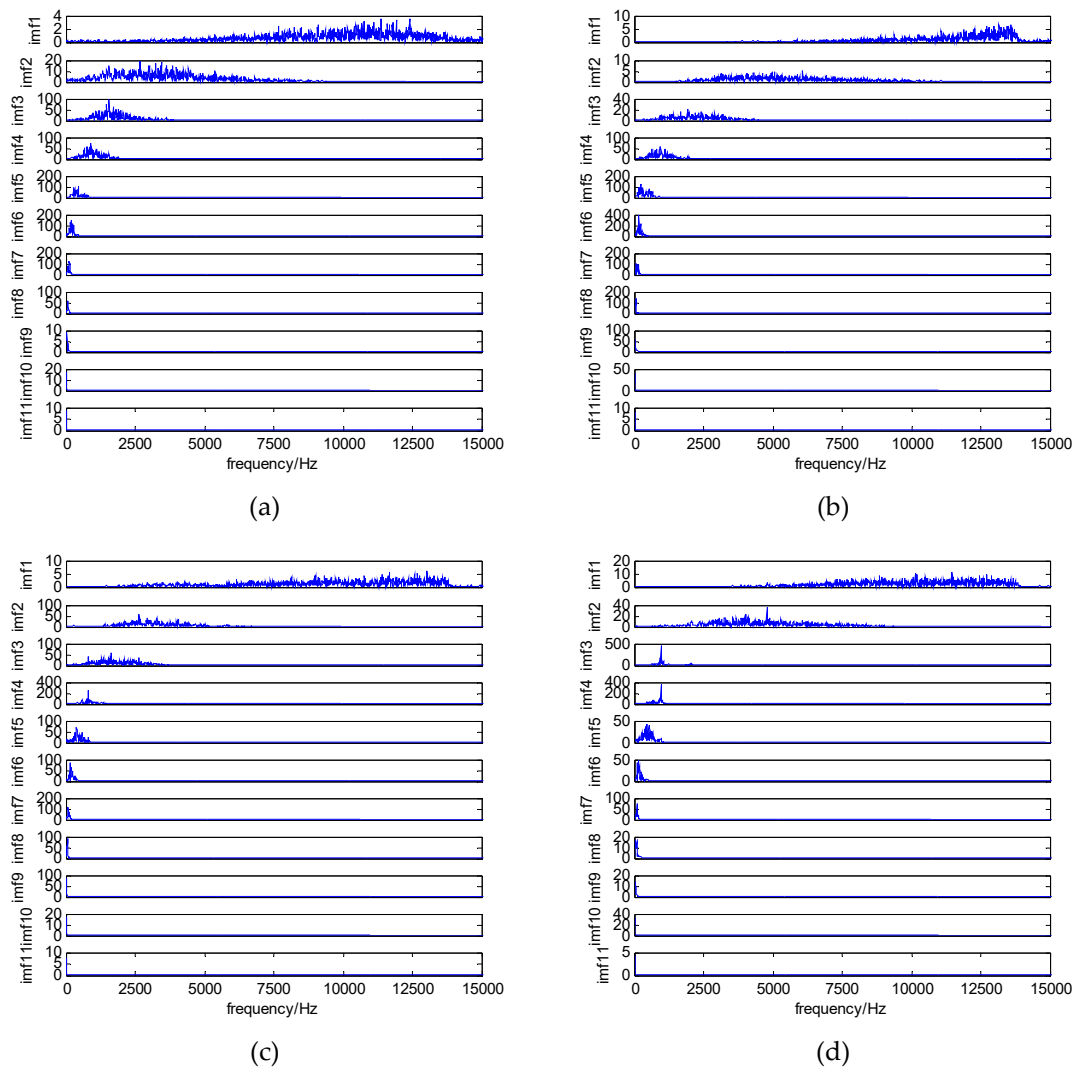


Figure 7. The IMF spectrum distribution by EEMD for four types of S-RN signals. (a) The first S-RN; (b) The second S-RN; (c) The third S-RN; (d) The fourth S-RN.

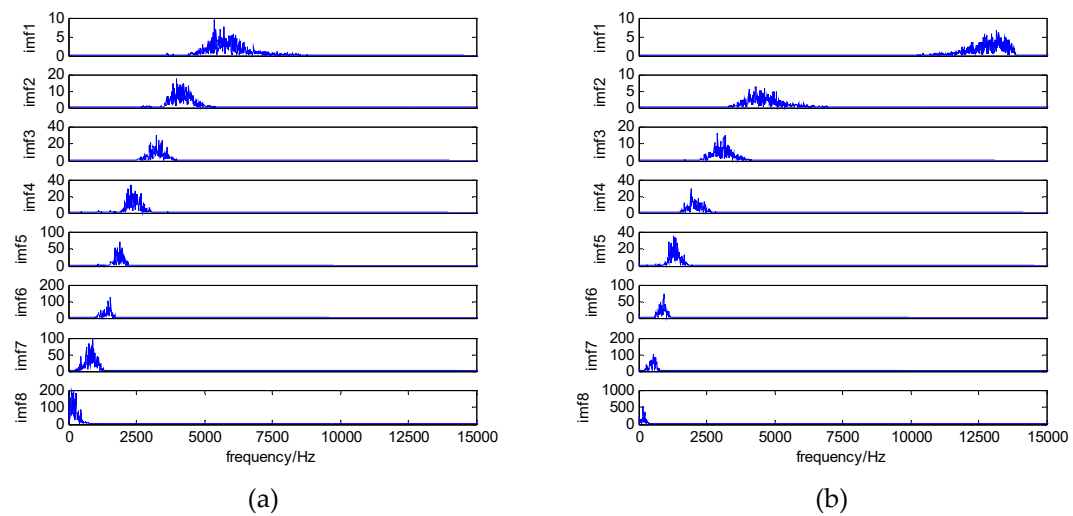


Figure 8. Cont.

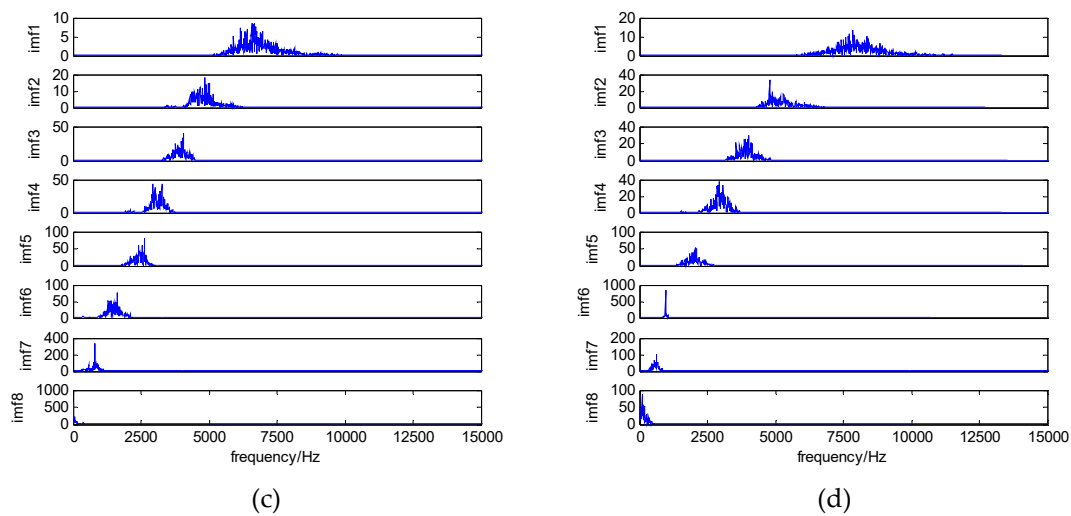


Figure 8. The IMF spectrum distribution by IVMD for four types of S-RN signals. (a) The first S-RN; (b) The second S-RN; (c) The third S-RN; (d) The fourth S-RN.

3.3. The Center Frequency Analysis

The center frequency of IMF is often regarded as the characteristic parameter of S-RN signal. IMF of four types of S-RN signals are obtained by EMD, EEMD and IVMD. The center frequency of each IMF can be calculated.

Figures 9–11 show the center frequency distribution of IMF by EMD, EEMD and IVMD respectively. For comparison, the first eight IMF from high to low frequency are selected for research. Figures 9a, 10a and 11a show the center frequency of IMF distribution in frequency descending by EMD. As can be seen from Figures 9a, 10a and 11a, there are significant differences in the center frequency of the high-frequency IMF of the four types, especially by VMD, while the difference of the low-frequency IMF is small. In Figures 9b, 10b and 11b, the center frequency of IMF distribution is arranged with descending levels of energy. It can be found that the main energy of four types is distributed in the low-frequency IMF, and the high-frequency IMF occupy a small proportion. In summary, the center frequency of high-frequency IMF have some obvious differences, however it cannot represent the main characteristics of S-RN signal because of its low energy. According to the data of literature [23], this article chooses the maximum energy IMF (EIMF) to represent the main characteristics of the original S-RN signal.

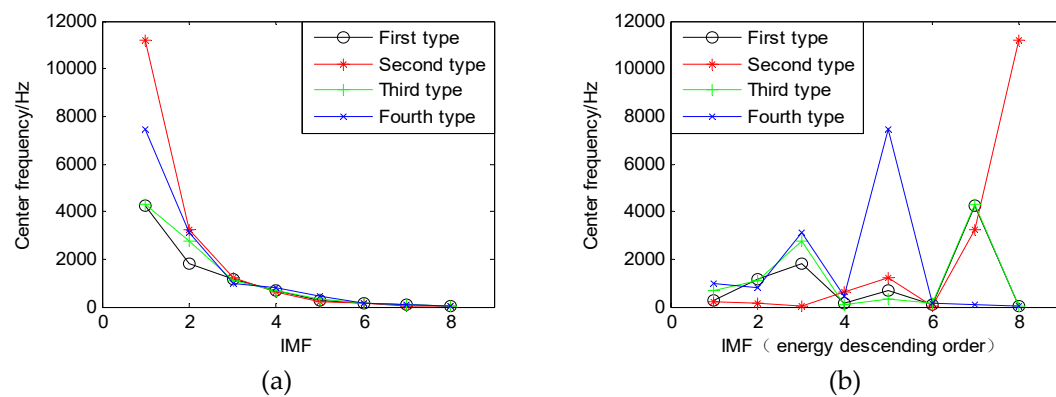


Figure 9. Center frequency of IMF by EMD for four types of S-RN signals. (a) The center frequency of IMF distribution with frequency descending; (b) the center frequency of IMF distribution with energy descending.

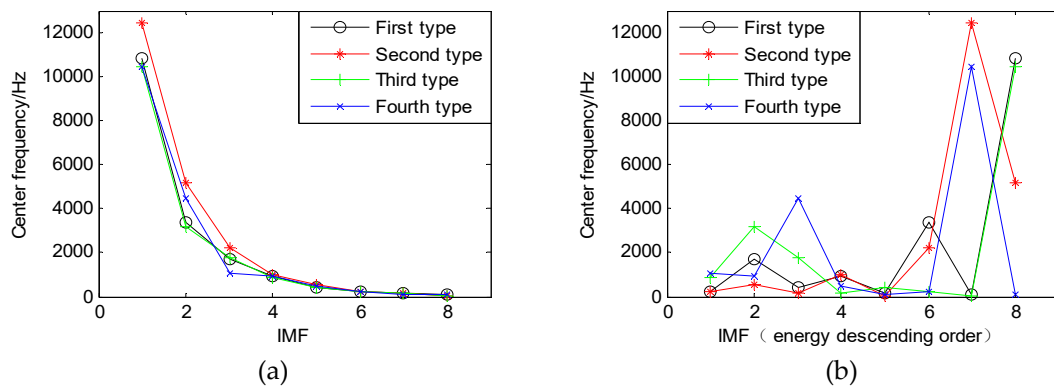


Figure 10. The center frequency of IMF by EEMD for four types of S-RN signals. (a) The center frequency of IMF distribution with frequency descending; (b) the center frequency of IMF distribution with energy descending.

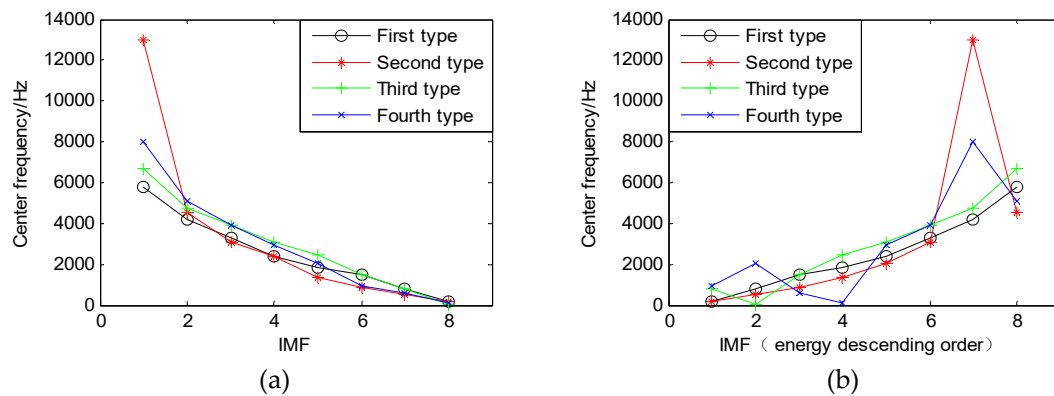


Figure 11. Center frequency of IMF by IVMD for four types of S-RN signals. (a) The center frequency of IMF distribution with frequency descending; (b) the center frequency of IMF distribution with energy descending.

Table 5 further shows the center frequency distribution of four types of EIMF. There is some difference in the center frequency of EIMF, the difference between the third and fourth types is obvious, while the center frequency of EIMF is close for the first and second types. The EIMF of the first and the second types are all at the same level, which is the key reason for the similar frequencies.

Table 5. The center frequency of the EIMF for four types of S-RN signals.

		EMD	EEMD	IVMD
First type	EIMF (level)	5	6	8
	Center frequency	262.52	223.6	186.73
Second type	EIMF (level)	5	6	8
	Center frequency	205.7	199.29	164.18
Third type	EIMF (level)	4	4	7
	Center frequency	702.79	839.24	795.88
Fourth type	EIMF (level)	3	3	6
	Center frequency	991.65	1092.6	967.98

3.4. The SE analysis

Consistent with Figures 9–11, Figures 12–14 shows the SE distribution of IMF by EMD, EEMD and IVMD respectively. Figures 12a, 13a and 14a shows the SE of the first eight IMF distribution with the

frequency descending. As can be seen from Figures 12a, 13a and 14a, there are significant differences in the SE of the high-frequency IMF of the four types, while the difference of the low-frequency IMF is small. In Figures 12b, 13b and 14b the SE of IMF distribution are arranged with the energy descending, and the difference of SE is more obvious than in Figures 12a, 13a and 14a. In Figure 14b, it can be found that the larger the SE is, the smaller the energy of IMF is.

SE of EIMF is chosen as the characteristic parameter, and the SE of EIMF distribution for four types is shown in Table 6. As can be seen from Table 6, the SE of EIMF obtained by the three decomposition methods are different, however the difference is small, especially for the first and second types.

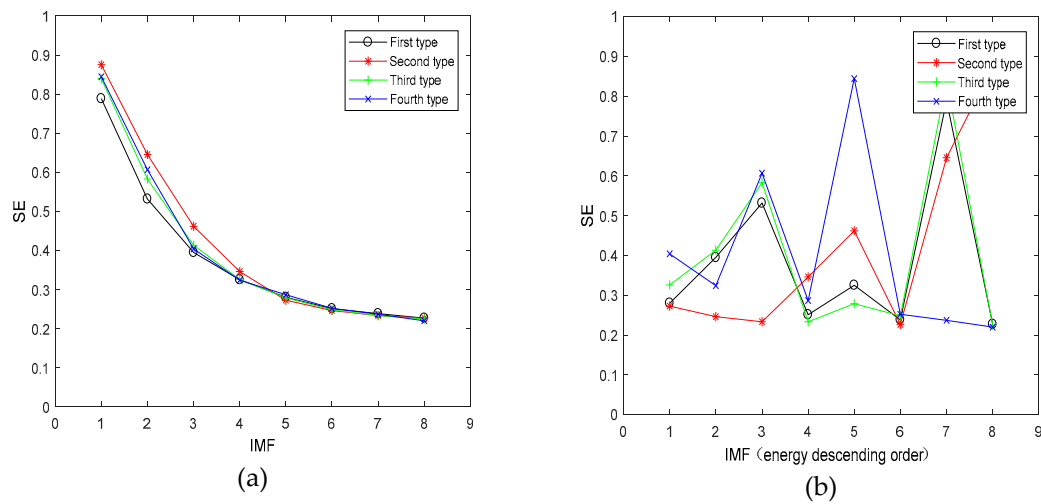


Figure 12. SE of IMF by EMD for four types of S-RN signals. (a) The SE of IMF distribution with frequency descending; (b) the SE of IMF distribution with energy descending.

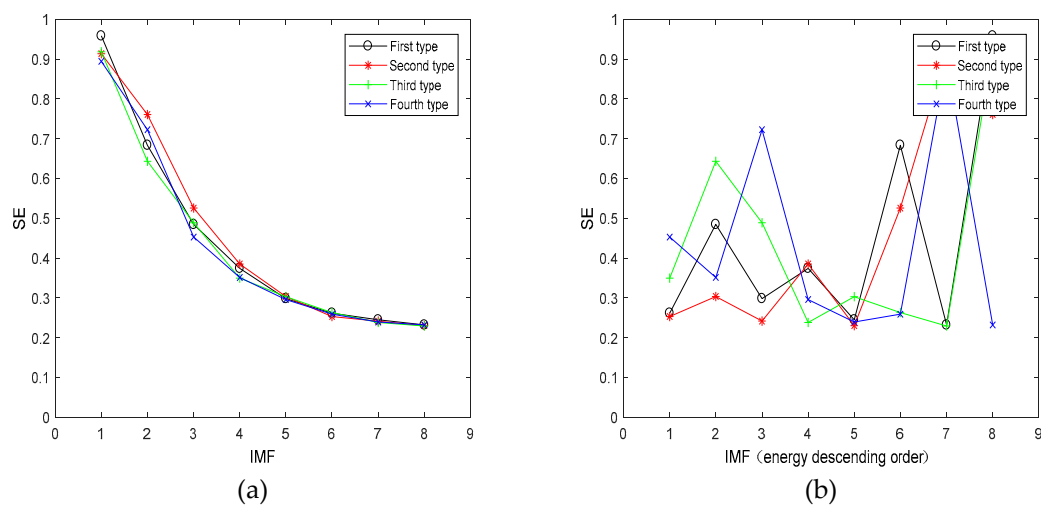


Figure 13. SE of IMF by EEMD for four types of S-RN signals. (a) The SE of IMF distribution with frequency descending; (b) the SE of IMF distribution with energy descending.

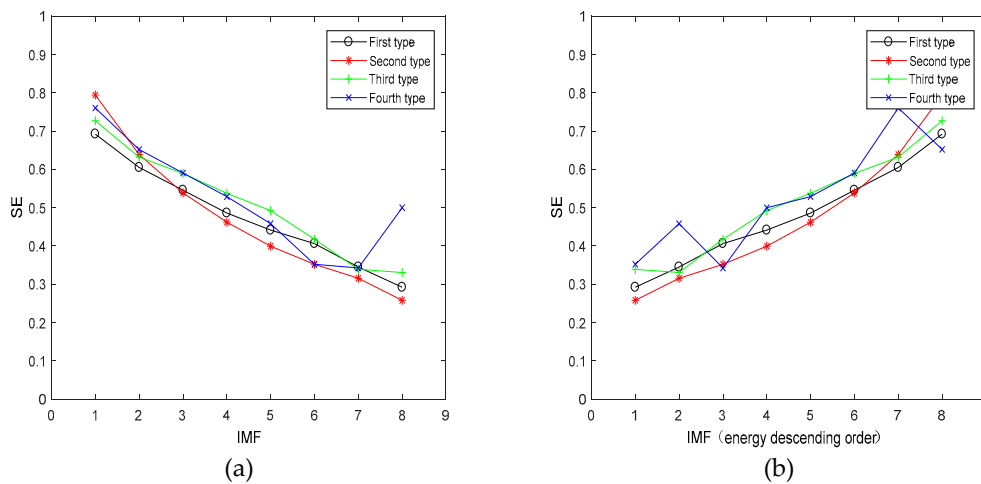


Figure 14. SE of IMF by IVMD for four types of S-RN signals. (a) The SE of IMF distribution with frequency descending; (b) the SE of IMF distribution with energy descending.

Table 6. The SE of the EIMF for four types of S-RN signals.

		EMD	EEMD	IVMD
First type	EIMF (level)	5	6	8
	SE	0.28013	0.26173	0.29225
Second type	EIMF (level)	5	6	8
	SE	0.27281	0.2533	0.25808
Third type	EIMF (level)	4	4	7
	SE	0.32573	0.34958	0.339
Fourth type	EIMF (level)	3	3	6
	SE	0.40386	0.45298	0.3521

4. Comparison of Feature Extraction Methods

In order to verify the universality of the difference between the four types of S-RN signal, 20 samples were randomly selected for each type to calculate the center frequency and SE of EIMF by EMD, EEMD and IVMD respectively. Figure 15 shows the center frequency distribution of the EIMF by the three decomposition methods with 20 samples for each type. Unlike Figure 15, Figure 16 shows the SE distribution. It is discovered that the center frequency of EIMF are at the same level for similar ships, however, there are differences for different types of ships. The center frequency of EIMF obtained by the IVMD has better robustness. The three decomposition methods can distinguish the third and the fourth types of S-RN signals, however, due to the similar center frequency of the EIMF for the first and second type, the method based on the center frequency of EIMF cannot effectively distinguish the four types of S-RN signals.

SE of EIMF by EMD and EEMD can distinguish the third and fourth types, while SE of EIMF for the first and second types too similar to distinguish from each other in Figure 16. Otherwise, the SE of EIMF by IVMD for four types of S-RN signal is obviously different.

In order to verify the validity of the method based on IVMD and SE of EIMF. Table 7 shows the average, standard deviation (SD) and range of the SE of EIMF for the four types of S-RN signals under the three decomposition methods with 20 samples each type. As can be seen in Table 7, the mean value of SE of EIMF for the four types by IVMD is obviously different, and their fluctuation range is not overlapping. However, for the first and second types, the mean value is so similar, and their range is overlapping by the EMD and EEMD method; the SD obtained by the EEMD method is less than that obtained by EMD, and the SD obtained by IVMD method is less than EEMD for the third and fourth types. Compared with EMD and EEMD methods, the proposed method can better distinguish the four types of S-RN signals.

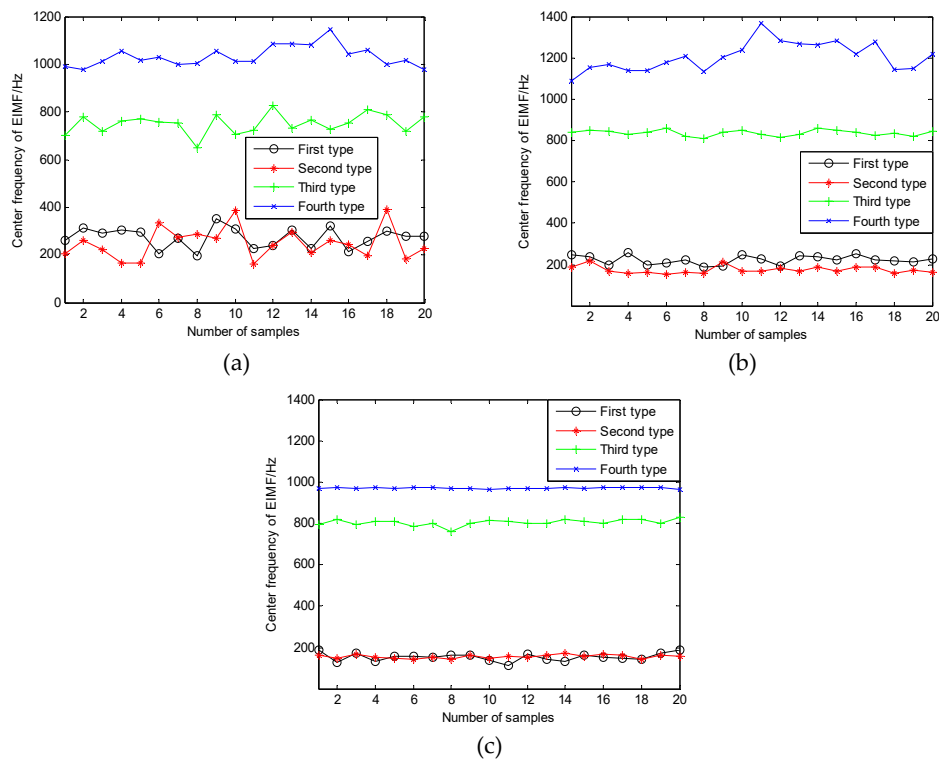


Figure 15. Center frequency distribution of the EIMF for four types of S-RN signals. (a) EMD; (b) EEMD; (c) IVMD.

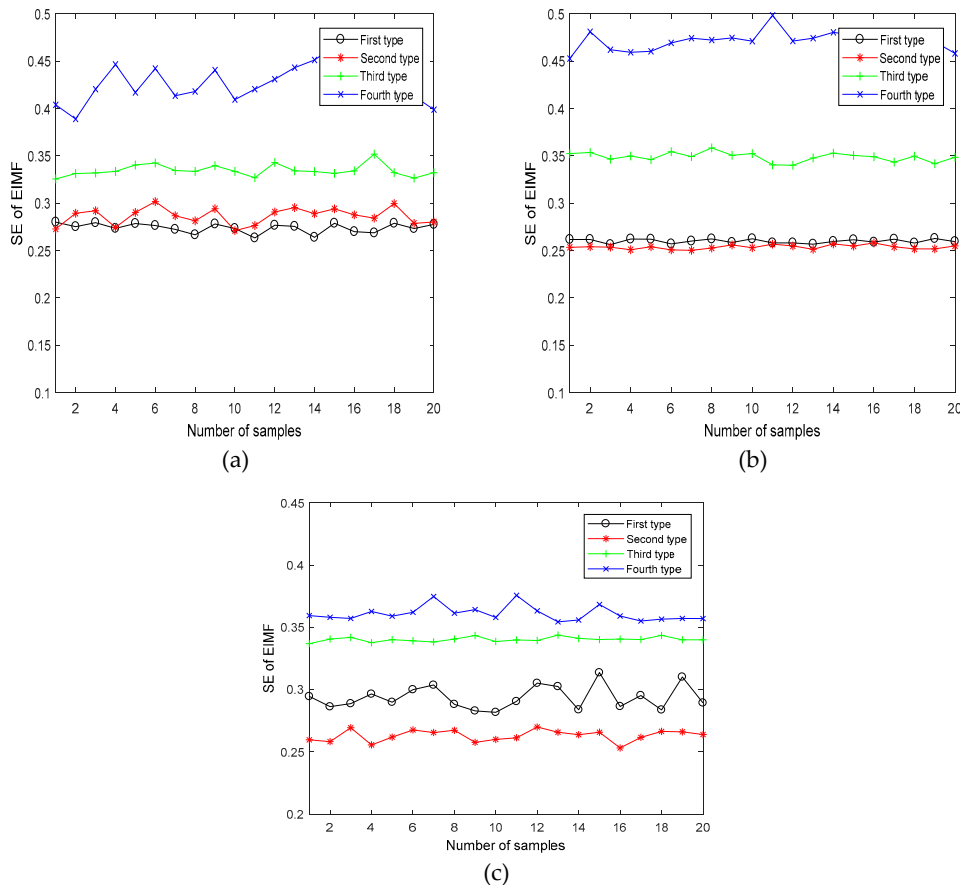


Figure 16. SE distribution of the EIMF for four types of S-RN signals. (a) EMD; (b) EEMD; (c) IVMD.

Table 7. The statistical characteristics of SE of the EIMF for four types of S-RN signals.

		EMD	EEMD	IVMD
First type	average	0.2741	0.26	0.2937
	SD	0.0051	0.0022	0.0094
	range	0.2634–0.2801	0.2563–0.2628	0.2818–0.3136
Second type	average	0.2865	0.2537	0.2631
	SD	0.0088	0.0022	0.0046
	range	0.2711–0.3017	0.2504–0.2582	0.2532–0.2702
Third type	average	0.3347	0.3489	0.3403
	SD	0.0062	0.0048	0.0018
	range	0.3257–0.3518	0.3401–0.3585	0.3369–0.3438
Fourth type	average	0.4255	0.4715	0.3609
	SD	0.0191	0.0105	0.0062
	range	0.3889–0.4661	0.4528–0.4983	0.3544–0.3757

5. Conclusions

IVMD as a novel algorithm combining SE is first proposed for feature extraction of S-RN signals. The selection of parameters is the key problem in IVMD. At first, according to the priori characteristics of S-RN signal and the analysis of experimental data, the main parameters are fixed in an orderly manner. Then four types of S-RN signals are decomposed by EMD, EEMD and IVMD, by analyzing and comparing the center frequency and the SE of IMF, it is found that the center frequency and the SE of IMF are similar for the same type of S-RN signal, while showing difference for different ones. Simulation results show the SE of EIMF by IVMD is more different than other methods for four types of S-RN signals.

Based on the above results, the SE of EIMF by IVMD is selected as a novel feature for the S-RN signal. Compared with the center frequency and SE of the EIMF by EMD and EEMD, the proposed method can represent the complexity of the EIMF of S-RN signals, and has a better distinguishing ability than the existing ones. Consequently, the novel method also can be used as the basis of classification and recognition.

Author Contributions: Y.L. contributed the feature extraction method, all authors designed and analyzed the experiments.

Funding: Authors gratefully acknowledge the supported by National Natural Science Foundation of China (No. 51409214 and No. 51179157) and Key Research and Development Program of Shaanxi province (2018NY-127).

Conflicts of Interest: The authors declare no conflict of interest.

References

1. Yang, D.; Liao, W.; Wang, Y.; Zeng, K.; Chen, Q.; Li, D. Data-Driven Optimization Control for Dynamic Reconfiguration of Distribution Network. *Energies* **2018**, *11*, 2628. [[CrossRef](#)]
2. Bustos, A.; Rubio, H.; Castejon, C.; Garcia-Prada, J.C. Condition monitoring of critical mechanical elements through Graphical Representation of State Configurations and Chromogram of Bands of Frequency. *Measurement* **2019**, *135*, 71. [[CrossRef](#)]
3. Vилlecco, F. On the Evaluation of Errors in the Virtual Design of Mechanical Systems. *Machines* **2018**, *6*, 36. [[CrossRef](#)]
4. Urick, R.J. *Principles of Underwater Sound*, 3rd ed.; McGraw-Hill: New York, NY, USA, 1983.
5. Siddagangaiah, S.; Li, Y.; Guo, X.; Yang, K. On the dynamics of ocean ambient noise: Two decades later. *Chaos* **2015**, *25*, 103117. [[CrossRef](#)] [[PubMed](#)]
6. Huh, J.-H.; Koh, T.; Seo, K. Design of a Shipboard Outside Communication Network and Its Testbed Using PLC: For Safety Management during the Ship Building Process. *Processes* **2018**, *6*, 67. [[CrossRef](#)]

7. Li, Y.; Li, Y.; Chen, X.; Yu, J.; Yang, H.; Wang, L. A New Underwater Acoustic Signal Denoising Technique Based on CEEMDAN, Mutual Information, Permutation Entropy, and Wavelet Threshold Denoising. *Entropy* **2018**, *20*, 563. [[CrossRef](#)]
8. Huang, N.E.; Shen, Z.; Long, S.R.; Wu, M.C.; Shih, H.H.; Zheng, Q.; Yen, N.C.; Tung, C.C.; Liu, H.H. The empirical mode decomposition and the Hilbert spectrum for nonlinear and non-stationary time series analysis. *Proc. R. Soc. Lond. A* **1998**, *454*, 903–995. [[CrossRef](#)]
9. Bustos, A.; Rubio, H.; Castejón, C.; García-Prada, J.C. EMD-Based Methodology for the Identification of a High-Speed Train Running in a Gear Operating State. *Sensors* **2018**, *18*, 793. [[CrossRef](#)]
10. Gao, B.; Woo, W.L.; Dlay, S.S. Single Channel Blind Source Separation Using EMD-Subband VariableRegularized Sparse Features. *IEEE Trans. Audio Speech Lang. Process.* **2011**, *19*, 961. [[CrossRef](#)]
11. Wu, Z.; Huang, N.E. Ensemble empirical mode decomposition: A noise-assisted data analysis method. *Adv. Adapt. Data Anal.* **2009**, *1*, 1. [[CrossRef](#)]
12. Li, Y.; Li, Y.; Chen, X.; Yu, J. A Novel Feature Extraction Method for Ship-Radiated Noise Based on Variational Mode Decomposition and Multi-Scale Permutation Entropy. *Entropy* **2017**, *19*, 342. [[CrossRef](#)]
13. Dragomireskiy, K.; Zosso, D. Variational mode decomposition. *IEEE Trans. Signal Process.* **2014**, *62*, 531–544. [[CrossRef](#)]
14. Liu, T.; Luo, Z.; Huang, J.; Yan, S. A Comparative Study of Four Kinds of Adaptive Decomposition Algorithms and Their Applications. *Sensors* **2018**, *18*, 2120. [[CrossRef](#)] [[PubMed](#)]
15. Li, Y.; Li, Y.; Chen, X.; Yu, J. Research on ship-radiated noise denoising using secondary variational mode decomposition and correlation coefficient. *Sensors* **2018**, *18*, 48. [[CrossRef](#)] [[PubMed](#)]
16. Li, Y.; Li, Y.; Chen, X.; Yu, J. Denoising and Feature Extraction Algorithms Using NPE Combined with VMD and Their Applications in Ship-Radiated Noise. *Symmetry* **2017**, *9*, 256. [[CrossRef](#)]
17. Liao, Y.; He, C.; Guo, Q. Denoising of Magnetocardiography Based on Improved Variational Mode Decomposition and Interval Thresholding Method. *Symmetry* **2018**, *10*, 269. [[CrossRef](#)]
18. Deng, W.; Liu, H.; Zhang, S.; Liu, H.; Zhao, H.; Wu, J. Research on an Adaptive Variational Mode Decomposition with Double Thresholds for Feature Extraction. *Symmetry* **2018**, *10*, 684. [[CrossRef](#)]
19. Richman, J.S.; Moorman, J.R. Physiological time-series analysis using approximate entropy and sample entropy. *Am. J. Physiol Heart Circ. Physiol.* **2000**, *278*, 2039. [[CrossRef](#)]
20. Bandt, C.; Pompe, B. Permutation entropy: A natural complexity measure for time series. *Phys. Rev. Lett.* **2002**, *88*, 174102. [[CrossRef](#)]
21. Rucco, M.; Gonzalez-Diaz, R.; Jimenez, M.J.; Atienza, N.; Cristalli, C.; Concettoni, E.; Ferrante, A.; Merelli, E. A new topological entropy-based approach for measuring similarities among piecewise linear functions. *Signal Process.* **2017**, *134*, 130–138. [[CrossRef](#)]
22. Zhang, X.; Liang, Y.; Zhou, J.; Zhou, J.; Zang, Y. A novel bearing fault diagnosis model integrated permutation entropy, ensemble empirical mode decomposition and optimized SVM. *Measurement* **2015**, *69*, 164. [[CrossRef](#)]
23. Yin, A.; Zhao, L.; Gao, B.; Woo, W.L. Fast partial differential equation de-noising filter for mechanical vibration signal. *Math. Methods Appl. Sci.* **2015**, *38*, 4879–4890. [[CrossRef](#)]
24. Chin, C.S.; Ji, X.; Woo, W.L.; Kwee, T.J.; Yang, W. Modified multiple generalized regression neural network models using fuzzy C-means with principal component analysis for noise prediction of offshore platform. *Neural Comput. Appl.* **2017**, *6*, 1–16. [[CrossRef](#)]
25. Tripathy, R.K.; Paternina, M.R.A.; Arrieta, J.G.; Pattanaik, P. Automated detection of atrial fibrillation ECG signals using two stage VMD and atrial fibrillation diagnosis index. *J. Mech. Med. Biol.* **2017**, *17*, 840–844.
26. Li, Y.; Li, Y.; Chen, Z.; Chen, X. Feature Extraction of Ship-Radiated Noise Based on Permutation Entropy of the Intrinsic Mode Function with the Highest Energy. *Entropy* **2016**, *18*, 393. [[CrossRef](#)]
27. Zhou, J.; Sun, N.; Jia, B.; Peng, T. A Novel Decomposition-Optimization Model for Short-Term Wind Speed Forecasting. *Energies* **2018**, *11*, 1752. [[CrossRef](#)]
28. Shang, H.; Lo, K.L.; Li, F. Partial Discharge Feature Extraction Based on Ensemble Empirical Mode Decomposition and Sample Entropy. *Entropy* **2017**, *19*, 439. [[CrossRef](#)]

